Progress of Theoretical Physics, Vol. 128, No. 5, November 2012

Quark-Anti-Quark Potentials from Nambu-Bethe-Salpeter Amplitudes on Lattice

Yoichi IKEDA[1,2] and Hideaki IIDA[3]

[1]*Department of Physics, Tokyo Institute of Technology, Tokyo 152-8551, Japan*
[2]*RIKEN Nishina Center, Wako 351-0198, Japan*
[3]*Department of Physics, Kyoto University, Kyoto 606-8502, Japan*

(Received December 26, 2011; Revised September 9, 2012)

Quark–anti-quark ($\bar{q}$-q) potentials with finite quark masses are studied from the $\bar{q}$-q Nambu-Bethe-Salpeter (NBS) wave functions in quenched lattice QCD. With the use of a method which has been recently developed in the derivation of nuclear forces from lattice QCD, we derive the $\bar{q}$-q potentials from the NBS wave functions. We calculate the $\bar{q}$-q NBS wave functions in pseudo-scalar and vector channels for several quark masses. The derived potentials at each quark mass in both channels show linear plus Coulomb form. We also discuss the quark-mass and channel dependence of the $\bar{q}$-q potentials.

Subject Index: 164, 232

§1. Introduction

An inter-quark potential is one of the most important ingredients of quantum chromodynamics (QCD). Experimentally, Regge slope[1)] suggests that the inter-quark potentials show linear behavior at long distance. The string tension of the potentials between a quark and an anti-quark, $\sigma \simeq 1.3$ GeV/fm, can be roughly estimated by mass spectra of hadrons using the relation $J = M^2/(4\sigma)$ with the spin J and the mass M of hadrons. At short distance, the inter-quark potential shows like the Coulomb interaction, which is, for example, suggested by the analogy between quarkonium and positronium. In fact, the linear plus Coulomb behaviors of the inter-quark potentials reproduce the low-lying hadron spectra well in quark models.

Theoretically, the study of the inter-quark potentials is challenging issue due to the non-perturbative nature of low energy phenomena in QCD. Lattice QCD simulation is the powerful tool for a numerical investigation in such a strong-coupling region of QCD. From the expectation value of the Wilson loops, the potential for an infinitely heavy quark and anti-quark ($\bar{Q}$-Q potential) and also the three-quark potential ($3Q$ potential) can be obtained on lattices.[2),3)] The $\bar{Q}$-Q potential from quenched lattice QCD simulations reveals the form of $V(r) = \sigma r - A/r + C$ with $\sigma = 0.92$ GeV/fm and $A = 51$ MeV·fm.[2)–5)]

The actual inter-quark potentials suffer from the effect of quark motions, which is not included in the $\bar{Q}$-Q potential. One can take into account the corrections coming from finite quark masses m_q order by order with the use of the heavy quark effective field theory. The effective field theory utilizes the hierarchy of scales coming from the heavy quark mass m_q and the relative velocity of heavy quarks, v. The potential nonrelativistic QCD (pNRQCD) is such an effective field theory at the

ultrasoft scale $m_q v^2$ obtained by integrating out the hard scale m_q and the soft scale $m_q v$.[2),6)–9)] It is convenient to employ pNRQCD to obtain the corrections of heavy quarkonium spectra to the heavy quark motion.

On the other hand, one can also study the mass spectra of mesons with phenomenological models of constituent quarks. In the constituent quark models, the potential between a quark and an anti-quark is usually parametrized by the Coulomb plus linear confinement force and spin-dependent terms expected by one-gluon exchange. With this potential, the constituent quark models well reproduce the mass spectra in wide energy region (see, e.g., Ref. 10)) and are commonly used for the studies of hadron structures. However, since such a phenomenological parametrization of the potentials affects interpretations of hadron structures, the derivation of the quark model potential from QCD is an important issue. In this work, we study potentials between a quark and an anti-quark with a finite mass ($\bar{q}$-q potentials) from quenched lattice QCD simulations. In order to explore the $\bar{q}$-q potentials, we apply the systematic method which utilize the equal-time Nambu-Bethe-Salpeter (NBS) amplitudes to extract hadronic potentials[11)–23)] to the $\bar{q}$-q systems with finite quark masses. Due to the absence of the asymptotic fields of quarks, the reduction formula cannot be applied directly. Therefore, we assume that the equal-time NBS amplitudes for the $\bar{q}$-q systems satisfy the Nambu-Bethe-Salpeter (NBS) equation with constant quark masses which could be considered as the constituent quark masses. By using the derivation of the relativistic three-dimensional formalism from the NBS equation developed by Lévy, Klein and Macke (LKM formalism),[25)–28)] we shall obtain the $\bar{q}$-q potentials *without expansion in terms of* m_q. The preliminary results of the NBS wave functions and potentials of the $\bar{q}$-q systems have been reported in Ref. 29).

The paper is organized as follows. In §2, we present our method to extract the $\bar{q}$-q potentials. In §3, we show the lattice QCD setup. We then show our numerical results of the $\bar{q}$-q wave functions and potentials in pseudo-scalar and vector channels for four different quark masses in §4. The obtained potentials reveal the linear plus Coulomb forms which are similar to the $\bar{Q}$-Q potential from the Wilson loop. We perform fitting analyses of the $\bar{q}$-q potential data. Section 5 is devoted to discussion and a summary.

§2. Method of the extraction of inter-quark potentials

Following the formulation to define the potentials on lattices,[11),12),27)] we show the basic equations to extract the $\bar{q}$-q potentials on the lattice below. As shown in Ref. 27), the equal-time choice of the Nambu-Bethe-Salpeter (NBS) amplitudes satisfies the relativistic Schrödinger-type equation *without an instantaneous approximation* for original interaction kernels of the NBS equation. Therefore, we can start with the Schrödinger-type equation (which is referred to as LKM equation in Ref. 27)) for the NBS wave function $\phi(\vec{r}; J^\pi)$ in the spin-parity J^π channels to define

potentials:*)

$$-\frac{\nabla^2}{2\mu}\phi(\vec{r};J^\pi)+\int d\vec{r}\,'U(\vec{r},\vec{r'};J^\pi)\phi(\vec{r'};J^\pi)=E\phi(\vec{r};J^\pi), \tag{2·1}$$

where $\mu(=m_q/2)$ and $E(=M^2_{\rm meson}/4m_q-m_q)$ denote the reduced mass of the $\bar{q}$-q system and the non-relativistic energy, respectively, and we simply assume non-relativistic kinematics. Note that the potential $U(\vec{r},\vec{r}\,';J^\pi)$ is generally energy-independent and non-local.[12),24)] In Appendix A, we discuss potentials derived from the Schrödinger-type equation with relativistic kinematics. The relativistic effects may be necessary to reproduce the meson mass spectra in the wide energy region.

For the two-nucleon case, it is proved that the Schrödinger-type equation is derived by using the reduction formula.[12)] Due to the absence of asymptotic fields for confined quarks, we suppose that the $\bar{q}$-q systems satisfy the NBS equation with their constant quark masses. In this study, constant quark masses m_q are determined by half of vector meson masses M_V, i.e., $m_q=M_V/2$, as usually taken in constituent quark models. Then, one finds Schrödinger-type equation of Eq. (2·1) as a three-dimensional reduction of NBS equation by applying LKM[25)–28)] method.

The energy-independent and non-local potential $U(\vec{r},\vec{r'};J^\pi)$ can be expanded in powers of the relative velocity $\vec{v}=-i\nabla/\mu$ of $\bar{q}$-q systems at low energies,

$$\begin{aligned}U(\vec{r},\vec{r'};J^\pi)&=V(\vec{r},\vec{v};J^\pi)\delta(\vec{r}-\vec{r'})\\&=(V_{LO}(\vec{r};J^\pi)+V_{NLO}(\vec{r};J^\pi)+\cdots)\delta(\vec{r}-\vec{r'}),\end{aligned} \tag{2·2}$$

with

$$V_{LO}(\vec{r};J^\pi)=V_C(\vec{r})+V_T(\vec{r})S_{12}, \tag{2·3}$$

$$V_{NLO}(\vec{r};J^\pi)=V_{LS}(\vec{r})\vec{L}\cdot\vec{S}, \tag{2·4}$$

where the N^nLO term is of order $O(\vec{v}^n)$, and S_{12}, $\vec{L}$ and $\vec{S}$ being the tensor operator,**) orbital angular momentum and spin of the $\bar{q}$-q systems, respectively. Note that the velocity expansion is different from the usual $1/m_q$ expansion, and the central force $V_C(\vec{r})$ in the leading order potential includes not only linear plus Coulomb confinement interaction, $V_{\rm conf}(\vec{r})$, but also higher order terms in the $1/m_q$ expansion such as the spin-spin interaction, $V_{\rm spin}(\vec{r})\vec{\sigma}_{\bar{q}}\cdot\vec{\sigma}_q$, which is regarded as an order $O(1/m_q^2)$. This spin-spin interaction is an important ingredient of the mass formula in the constituent quark model. At the leading order, one finds

$$V(\vec{r};J^\pi)\simeq V_{LO}(\vec{r};J^\pi)=\frac{1}{2\mu}\frac{\nabla^2\phi(\vec{r};J^\pi)}{\phi(\vec{r};J^\pi)}+E. \tag{2·5}$$

The s-wave effective leading order $\bar{q}$-q potentials $V_{LO}(\vec{r};J^\pi)$ are studied in this work. As proposed in Ref. 21), we shall show both $V_{\rm conf}(\vec{r})$ and $V_{\rm spin}(\vec{r})$, which can be

*) In this paper, the three-dimensional interactions $U(\vec{r},\vec{r}\,';J^\pi)$ of the Schrödinger-type equation in Eq. (2·1) are referred to as potentials, which is faithful to the equal-time NBS amplitudes.

**) The tensor potential gives a coupling between s-wave and d-wave components in the vector meson channel.

constructed by

$$V_{\rm conf}(\vec{r}) - E_{\rm av} = \frac{1}{m_q}\left[\frac{1}{4}\frac{\nabla^2\phi(\vec{r};0^-)}{\phi(\vec{r};0^-)} + \frac{3}{4}\frac{\nabla^2\phi(\vec{r};1^-)}{\phi(\vec{r};1^-)}\right], \tag{2·6}$$

$$V_{\rm spin}(\vec{r}) - \Delta E = \frac{1}{m_q}\left[\frac{\nabla^2\phi(r;1^-)}{\phi(\vec{r};1^-)} - \frac{\nabla^2\phi(\vec{r};0^-)}{\phi(\vec{r};0^-)}\right], \tag{2·7}$$

with $E_{\rm av} = 1/4(E(0^-) + 3E(1^-))$ and $\Delta E = E(1^-) - E(0^-)$ to be determined by the energy eigenvalues in the pseudo-scalar and vector channels.

The convergence of the expansion of $\vec{v}$ can be checked by studying the energy dependence of the local potential $V_{LO}(\vec{r}; J^\pi)$ as in Ref. 15). When the local potential $V_{LO}(\vec{r}; J^\pi)$ has little energy dependence, the potential between $\bar{q}$-q is well described only by $V_{LO}(\vec{r}; J^\pi)$. In contrast, if the energy dependence is large, higher order terms are necessary. The study of the energy dependence of the local potential in the $\bar{q}$-q systems is an important future work.

In order to obtain the NBS wave functions of the $\bar{q}$-q systems on the lattice, let us consider the following equal-time NBS amplitudes:

$$\begin{aligned}\chi(\vec{x}+\vec{r},\vec{x},t-t_0;J^\pi) &= \langle 0|\,\bar{q}(\vec{x}+\vec{r},t)\Gamma q(\vec{x},t)\overline{\mathcal{J}}_{\bar{q}q}(t_0;J^\pi)\,|0\rangle \\ &= \sum_n A_n\,\langle 0|\,\bar{q}(\vec{x}+\vec{r},t)\Gamma q(\vec{x},t)\,|n\rangle\;\; e^{-M_n(t-t_0)},\end{aligned} \tag{2·8}$$

with the matrix elements

$$A_n = \langle n|\,\overline{\mathcal{J}}_{\bar{q}q}(t_0;J^\pi)\,|0\rangle\,. \tag{2·9}$$

Here Γ represents the Dirac γ-matrices, and $\overline{\mathcal{J}}_{\bar{q}q}(t_0;J^\pi)$ stands for the source term which creates the $\bar{q}$-q systems with spin-parity J^π on the lattice. The NBS amplitudes in Eq. (2·8) are dominated by the lowest mass state of mesons with the mass M_0 at large time separation ($t \gg t_0$):

$$\begin{aligned}\chi(\vec{r},t-t_0;J^\pi) &= \frac{1}{V}\sum_{\vec{x}}\chi(\vec{x}+\vec{r},\vec{x},t-t_0;J^\pi) \\ &\to A_0\phi(\vec{r};J^\pi)e^{-M_0(t-t_0)},\end{aligned} \tag{2·10}$$

with V being the volume of the box. Thus, the $\bar{q}$-q NBS wave functions are defined by the spatial correlation of the NBS amplitudes.

The NBS wave functions in s-wave states are obtained under the projection onto zero angular momentum ($P^{(l=0)}$),

$$\phi(\vec{r};J^\pi) = \frac{1}{24}\sum_{g\in O} P^{(l=0)}\phi(g^{-1}\vec{r};J^\pi), \tag{2·11}$$

where $g \in O$ represents 24 elements of the A_1 representation of the cubic rotational group,*) and the summation is taken for all these elements. Using Eqs. (2·5) and (2·11), we will find the $\bar{q}$-q potentials and NBS wave functions from lattice QCD.

*) The higher partial waves ($l \geq 4$) can couple to states in the A_1 representation, but such higher partial waves are exponentially suppressed.

Table I. Simulation parameters used in this work. Scale is set so as to reproduce the string tension, $\sqrt{\sigma} = 427$ MeV, from the expectation value of the Wilson loop.[3),5)]

β	a	lattice size	volume	$N_{\rm conf}$
6.0	0.104 fm	$32^3 \times 48$	$(3.3\ {\rm fm})^3$	100

§3. Numerical setup of the lattice simulations

In this section, we show the actions and simulation parameters in this work. We employ the standard plaquette gauge action,

$$S_G[U] \equiv \frac{\beta}{N_c} \sum_{x,\mu,\nu} {\rm ReTr}\{1 - P_{\mu\nu}(x)\}, \tag{3·1}$$

with $\beta \equiv 2N_c/g^2$. The plaquette $P_{\mu\nu}$ is defined as

$$P_{\mu\nu} = U_\mu(x) U_\nu(x+\hat{\mu}) U_\mu^\dagger(x+\hat{\nu}) U_\nu^\dagger(x), \tag{3·2}$$

where $U_\mu(x)$ is a link variable. As for quark fields $\psi(x)$, we adopt the standard Wilson fermion action,

$$S_F[\bar{\psi}, \psi, U] \equiv \sum_{x,y} \bar{\psi}(x) K(x,y) \psi(y), \tag{3·3}$$

$$K(x,y) \equiv \delta_{x,y} - \kappa \sum_\mu \{(\mathbf{1} - \gamma_\mu) U_\mu(x) \delta_{x+\hat{\mu},y} + (\mathbf{1} + \gamma_\mu) U_\mu^\dagger(y) \delta_{x,y+\hat{\mu}}\}, \tag{3·4}$$

where κ is the hopping parameter.

We generate the quenched gauge fields on a $32^3 \times 48$ lattice with QCD coupling $\beta = 6.0$, which corresponds to the physical volume $V = (3.3\ {\rm fm})^3$ and the lattice spacing $a = 0.104$ fm determined so as to reproduce the string tension, $\sqrt{\sigma} = 427$ MeV, from the expectation value of the Wilson loop.[3),5)] We measure the $\bar{q}$-q NBS wave functions for four different hopping parameters $\kappa = 0.1520, 0.1480, 0.1420, 0.1320$: the corresponding pseudo-scalar (PS) meson masses $M_{\rm PS}$ in the calculation are 0.94, 1.27, 1.77, 2.53 GeV, and vector (V) meson masses $M_{\rm V}$=1.04, 1.35, 1.81, 2.55 GeV, respectively. The number of configurations used in this simulation is 100 for each quark mass. The simulation parameters are summarized in Table I. The calculation of the $\bar{q}$-q NBS wave functions requires gauge fixing, because q and $\bar{q}$ operators are spatially separated at the sink time slice. Here we adopt Coulomb gauge, which is frequently used for studies of hadron spectroscopy in lattice QCD. As for the source operator of the $\bar{q}$-q systems, we employ a static wall source in Eq. (2·8),

$$\overline{\mathcal{J}}_{\bar{q}q}(t_0; J^\pi) = \bar{Q}(t_0) \Gamma Q(t_0), \tag{3·5}$$

with the static wall quark operator

$$Q(t_0) \equiv \sum_{\vec{x}} \psi(\vec{x}, t_0). \tag{3·6}$$

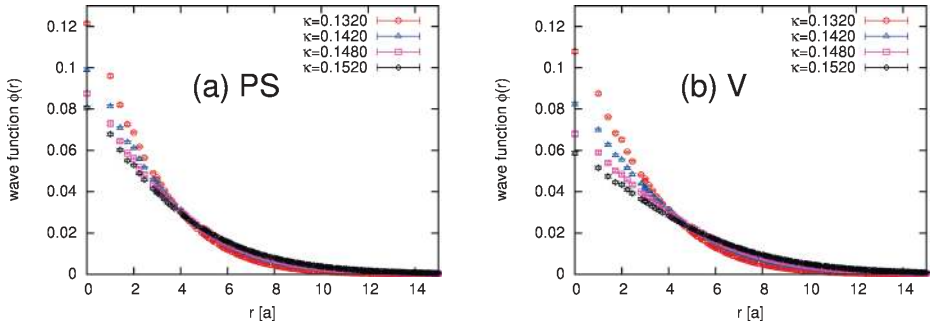

Fig. 1. The $\bar{q}$-q NBS wave functions in PS (a) and V (b) channels. The wave functions are normalized to be $\int d^3r\phi(\vec{r})\phi^*(\vec{r}) = 1$. All the wave functions are localized in the box and indicate the bound states.

Since the ground state saturations have been already achieved at time slice $t-t_0 = 20$, we shall show the NBS wave functions and the potentials at $t - t_0 = 20$.

We note that gauge fixings and sink operators can be arbitrary chosen in the formalism, and all potentials with different gauge fixings and sink operators give the same physical observables, i.e., mass spectra and scattering lengths for instance. In this work, we employ Coulomb gauge and a local operator for sink operators. We can take another gauge fixing and sink operator, and the potential obtained with these conditions is generally different from that obtained in this work. In Appendix B, we discuss the sink-operator dependence of the potential by using a gauge-invariant smeared operator for the sink.

§4. Numerical results for the $\bar{q}$-q potentials

First, we show the numerical results of the NBS wave functions in Fig. 1. Figures 1(a) and (b) are the NBS wave functions for each quark mass in PS and V channels, respectively. The NBS wave functions mostly vanish at $r = 1.5$ fm for all quark masses in both channels. This indicates that the spatial volume $V = (3.3 \text{ fm})^3$ is large enough for the present calculations. The size of a wave function with a lighter quark mass becomes larger than that with a heavier one. Comparing the results in PS and V channels, little channel dependence between PS and V channels is found, although the quark-mass dependence of the wave functions is a bit larger for V channel.

In Fig. 2, we show the Laplacian parts of $\bar{q}$-q potentials in Eq. (2·5), $\nabla^2\phi(r)/\phi(r)$, for each quark mass and channel. Figure 2(a) shows $\nabla^2\phi(r)/\phi(r) = 2\mu(V(r) - E)$ in PS channel for each quark mass. As shown in Fig. 2, one can see that the potential form is similar to that obtained from the Wilson loop, namely, that looks like linear plus Coulomb form, although the derivation of the potentials is largely different between these two methods. Figure 2(b) represents $\nabla^2\phi(r)/\phi(r)$ in V channel for each quark mass. The basic properties are similar to that in PS channel, although quark mass dependence is a bit larger for V channel.

Figures 3(a) and (b) show the potentials with the constant energy shifts E, i.e.,

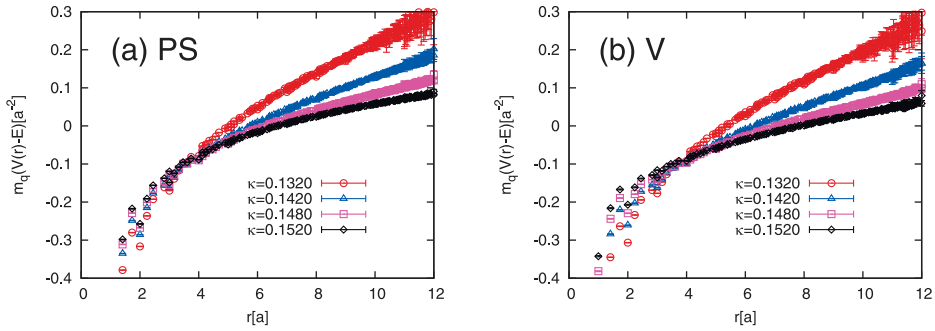

Fig. 2. Plots of $\nabla^2\phi(r)/\phi(r) = 2\mu(V(r) - E)$ in PS channel (a) and V channel (b) for each quark mass. The potentials show the linear plus Coulomb form.

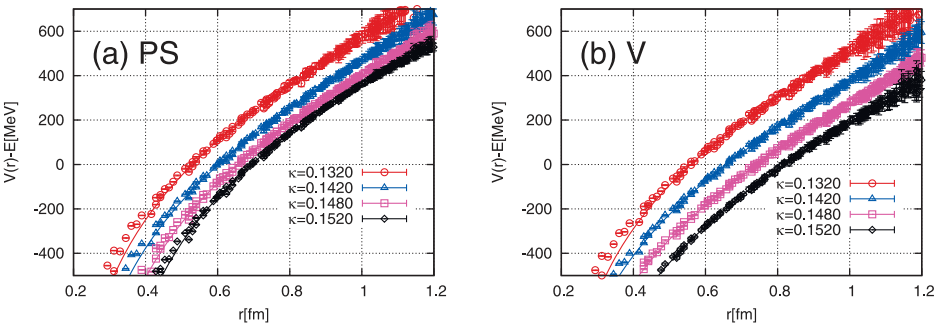

Fig. 3. Plots of the potential with the constant energy shift $V(r) - E = \nabla^2\phi(r)/(2\mu\phi(r))$ in PS channel (a) and V channel (b) for each quark mass. The solid curves are the fit function with linear plus Coulomb form shown in Table II.

$V(r) - E = \nabla^2\phi(r)/(2\mu\phi(r))$ in PS and V channels, respectively, for each quark mass. Note that the quark mass $m_q(= 2\mu)$ is determined by the half of vector meson mass, $m_q = M_V/2$, as mentioned in the previous section.

We perform fit analyses of the potentials in Figs. 3(a) and (b). For the fit function, we choose the linear plus Coulomb form, $f_1(r) = \sigma r - A/r + C$. We fit $f_1(r)$ to the potential data for each quark mass and channel. We use the on-axis data with the range $3 \leq r/a \leq 10$ in the fit.*) The fit results are summarized in Table II, and denoted by solid curves in Figs. 3(a) and (b). $\chi^2/N_{\rm df}$ is around 0.5 for all the fit, which means the data are well described by the linear plus Coulomb form. We find moderate quark mass dependence of the string tension. The string tension becomes larger as increasing quark masses in both channels, and that for heaviest quark mass in our simulation is about 820 MeV/fm, which is comparable to that obtained from an expectation value of the Wilson loop. On the other hand, the Coulomb coefficient A strongly depends on quark masses. The Coulomb coefficient becomes small as increasing quark masses, and is roughly approaching to that obtained from an expectation value of the Wilson loop.

*) In our preliminary analysis,[29] not only on-axis but also off-axis data are taken into account in the fit. Both data do not coincide due to the discretization error under the s-wave (A_1) projection.

Table II. The fitting results of the potentials in Fig. 3. The function to be fitted is $f_1(r) = \sigma(m_q, i)r - A(m_q, i)/r + C(m_q, i)$. The fit range is $3 \leq r/a \leq 10$.

	Pseudo-scalar			Vector		
κ	$\sigma(m_q, PS)$ MeV/fm	$A(m_q, PS)$ MeV·fm	$\chi^2/N_{\rm df}$	$\sigma(m_q, V)$ MeV/fm	$A(m_q, V)$ MeV·fm	$\chi^2/N_{\rm df}$
0.1320	819(47)	215(7)	0.32	825(48)	195(7)	0.63
0.1420	753(34)	264(5)	0.35	765(37)	216(6)	0.61
0.1480	691(30)	338(5)	0.46	723(39)	249(7)	0.44
0.1520	601(29)	443(5)	0.31	697(63)	291(13)	0.23

Table III. The fitting results of the potentials for $f_2(r)$ without the channel and the quark mass dependences of the string tension. The obtained string tension is $\sigma = 723(30)$ MeV/fm. The fit range is $3 \leq r/a \leq 10$.

	Pseudo-scalar	Vector
κ	$A(m_q, PS)$ MeV·fm	$A(m_q, V)$ MeV·fm
0.1320	231(5)	212(5)
0.1420	271(5)	225(5)
0.1480	332(5)	249(5)
0.1520	415(6)	285(7)

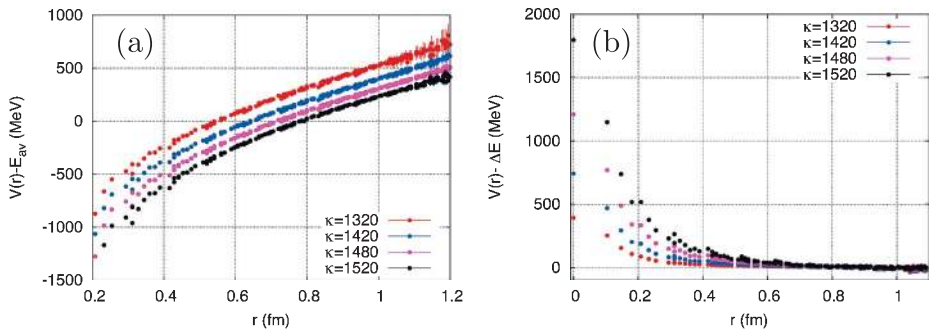

Fig. 4. (a) Spin-independent confinement potentials, $V_{\rm conf}(r) - E_{\rm av}$, and (b) spin-dependent potentials, $V_{\rm spin}(r) - \Delta E$.

Next, we perform another type of fit analysis. Assuming that the string tension σ is independent of the quark masses due to the quenched QCD simulations, where the contributions from quark loops are eliminated, we perform the fit by minimizing the general $\chi^2/N_{\rm df}$ which is defined as $\chi^2/N_{\rm df} = \sum_{m_q,i} \chi^2(m_q, i)/N_{\rm df}$ with $i = PS,\ V$.[30] We call the fit "universal fit" here. The fit function $f_2(r)$ can be explicitly written by $f_2(r) = \sigma r - A(m_q, i)/r + C(m_q, i)$. The free parameters of the fit are $\sigma, A(m_q, i)$, $C(m_q, i)$ for $f_2(r)$. In the fit, we choose the range of the potential data as $3 \leq r/a \leq 10$. The fitting results are shown in Table III. The general $\chi^2/N_{\rm df}$ is achieved with 1.52 for $f_2(r)$ with $\sigma = 723$ (30) MeV/fm. Since our simulation includes all the quark mass effects, $f_2(r)$ is modified by the higher order effect of $1/m_q$ expansion.

From the NBS wave functions in PS and V channels, we calculate the spin-

Table IV. The fitting results of the confinement potentials. The fitting function is chosen as the Cornell-type, $V(r) = \sigma r - A/r + C$.

κ	σ (MeV/fm)	A (MeV·fm)
0.1320	822(49)	200(7)
0.1420	766(38)	228(6)
0.1480	726(39)	269(7)
0.1520	699(57)	324(12)

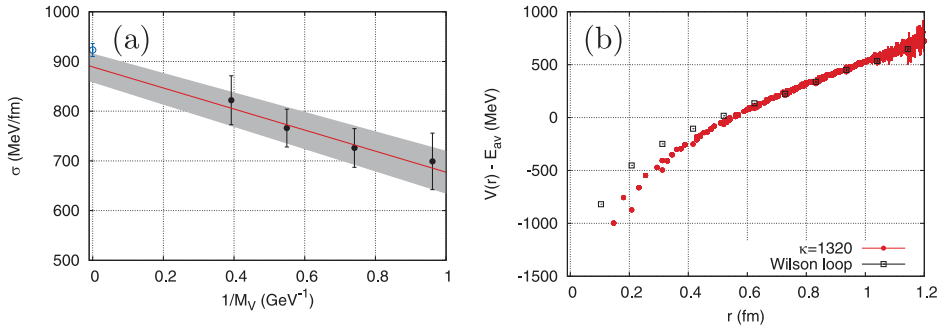

Fig. 5. (a) String tensions of the spin-independent potentials (filled circles) as a function of inverse vector meson masses $1/M_{\rm V}$. The string tension obtained from the Wilson loop is represented by open circle. The solid line denotes a linear extrapolation of the string tension to infinitely heavy quark mass limit together with 1σ error (shaded area). (b) Comparison of the spin-independent confinement potential (filled circle), $V_{\rm conf}(r) - E_{\rm av}$, for the heaviest quark mass ($\kappa = 0.1320$) with that obtained from the expectation value of the Wilson loop (open square).

independent and -dependent forces through Eqs. (2·6) and (2·7). In Fig. 4 (a), we show the spin-independent parts of the inter-quark potentials, while, in Fig. 4 (b), we show the spin-dependent potentials. The spin-independent potentials reveal the linear plus Coulomb confinement forces, and the spin-dependent potentials show short range repulsive interactions as expected from meson mass spectra.

We fit Cornell-type function, $V(r) = \sigma r - A/r + C$, to the spin-independent confinement potentials. The fitting results are summarized in Table IV. As expected in Table II, both the string tension and the Coulomb coefficient have the quark mass dependence. To compare our potential with the static potential, we extrapolate the quark mass dependent string tension to the infinitely heavy quark mass limit. Figure 5 (a) shows the string tension of the spin-independent confinement potentials as a function of the inverse vector meson mass, $1/M_{\rm V}$, and the solid line denotes a linear extrapolation to infinitely heavy quark mass limit. With this extrapolation, the string tension at the limit is 889(28) MeV/fm, which is consistent with that calculated from the Wilson loop (923(13) MeV/fm as in Ref. 5)) within the error denoted as shaded area in Fig. 5 (a). Figure 5 (b) shows the comparison of potentials in our approach with $\kappa = 0.1320$ with the static potential obtained from the expectation value of the Wilson loop. Both potentials coincide with each other at long distance, while a deviation is found at short distance. Several possibilities are considered for the deviation. One is the finite quark mass effects, because the higher

order terms in the $1/m_q$ expansion can contribute to short range interactions. The others are the artifact of discretization in the short range part of the potential and the definition of the constant quark mass adopted in this study. In Ref. 21), the relativistic heavy quark action and self-consistent determination of constant quark masses are employed, and both the linear and Coulomb coefficients at heavy quark limit are found to be consistent with Wilson loop analyses.

§5. Discussion and summary

We have studied the inter-quark potentials between a quark and an anti-quark ($\bar{q}$-q potentials) from the $\bar{q}$-q Nambu-Bethe-Salpeter (NBS) wave functions. For this purpose, we have utilized the method which has been recently developed in the calculation of nuclear force from QCD.[11),12)] We have calculated the NBS wave functions for the $\bar{q}$-q systems with four different quark masses in pseudo-scalar and vector channels and obtained the leading order $\bar{q}$-q potentials in the velocity expansion through the Schödinger-type equation. In this framework, the $\bar{q}$-q potentials basically contains full quark motions with the finite masses. As a result, we have found that the shapes of the $\bar{q}$-q potentials are the linear plus Coulomb form which is similar to the static $\bar{Q}$-Q potential obtained from the Wilson loop.

For the fitting, we have employed the Cornell-type function. We have found that both linear and Coulomb coefficients depend on the quark masses. We have also performed the linear extrapolation of the quark mass dependent string tension of the spin-independent potential to the heavy quark mass limit. As a result, we find that the extrapolated string tension obtained in this study is consistent with the static potential obtained from the Wilson loop. Our choice of constant quark masses, m_q, is rather phenomenological, and the Coulomb coefficient at heavy quark limit is larger than that of the static potential. Meanwhile, with the method presented in this paper, the self-consistent determination of the constant quark masses proposed in Ref. 21) gives a good agreement with the static potential. Therefore, this new approach to define the $\bar{q}$-q potential from NBS wave functions contains important properties of the Wilson loop.

This is the first step to study the $\bar{q}$-q potentials from the NBS wave functions, and we find that the obtained leading order $\bar{q}$-q potential in the velocity expansion has the basic property of that obtained from the Wilson loop. Therefore, this method will be useful for the study of the $\bar{q}$-q potentials and hadron spectroscopies with finite quark masses.

Acknowledgements

The authors thank S. Aoki, T. Doi, T. Hatsuda, T. Inoue, N. Ishii, K. Murano, H. Nemura, K. Sasaki, T. Kawanai and S. Sasaki for the fruitful discussion. Y. I. also thanks N. Kaiser, A. Laschka and W. Weise for the useful discussion. The calculations were performed mainly by using the NEC-SX9 and SX8R at Osaka University, and partly by RIKEN Integrated Cluster of Clusters (RICC) facility. This project is supported in part by a Grant-in-Aid for Japan Society for the Promotion

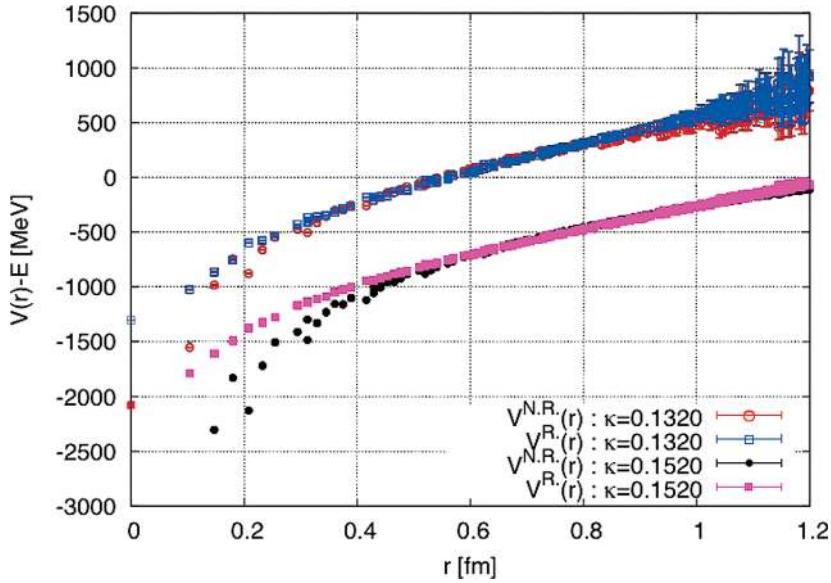

Fig. 6. Comparison of "relativistic" potentials $V^{\mathrm{R.}}(r)$ with non-relativistic potentials $V^{\mathrm{N.R.}}(r)$ shown in the main part.

of Science (No. 23-8687) and Scientific Research on Innovative Areas (Nos. 2004: 20105001, 20105003, 23105713).

Appendix A

—— *Inter-Quark Potential with Relativistic Kinematics* ——

In the main part of the paper, we assume the non-relativistic kinematics for the Schrödinger-type equation. Our aim here is to show the $\bar{q}$-q potentials with relativistic kinematics. Since the relativistic kinematics are used in the phenomenological constituent quark models[10] for the purpose to reproduce higher excited states, it is necessary to show how the change of the kinematics affects the shape of the potentials from lattice QCD.

The Schrödinger-type equation with relativistic kinematics for the $\bar{q}$-q system in the continuum limit is written as

$$\int d^3r' \left[\int \frac{d^3p'}{(2\pi)^3} 2\sqrt{\vec{p}'^2 + m_q^2} e^{-i\vec{p}'\cdot(\vec{r}-\vec{r}')} \right] \phi(\vec{r}'; J^\pi) + V(\vec{r}; J^\pi)\phi(\vec{r}; J^\pi) = E\phi(\vec{r}; J^\pi), \tag{A·1}$$

with the leading order potential $V(\vec{r}; J^\pi)$ of the velocity expansion and the relativistic energy $E = M_{\mathrm{meson}} - 2m_q$. On the lattice, a discrete Fourier transformation of $\vec{r}$ gives $\sin(\vec{p})$. Thus, $\sqrt{\vec{p}^2 + m_q^2}$ is replaced by $\sqrt{\sin^2(\vec{p}) + m_q^2}$, and the integral becomes a summation on the lattice. Similar as the procedure in the main part, we obtain the potential from the discretized version of the Schrödinger-type equation of Eq. (A·1).

Figure 6 is a comparison of the s-wave potentials in V channel with relativistic

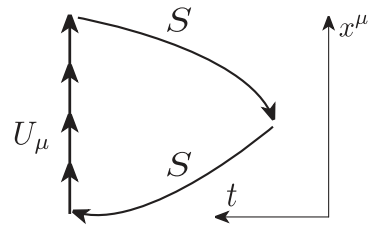

Fig. 7. Schematic figure of gauge-invariant smeared operator.

kinematics, $V^{\mathrm{R.}}(r)$, and non-relativistic potential, $V^{\mathrm{N.R.}}(r)$, shown in the main part. The relativistic potentials for $\kappa = 0.1320$ ($\kappa = 0.1520$) are shown by open square (filled square) in Fig. 6, while the non-relativistic potentials for $\kappa = 0.1320$ ($\kappa = 0.1520$) are shown by open circle (filled circle). As shown in Fig. 6, $V^{\mathrm{R.}}(r)$ again shows the linear plus Coulomb behavior, and $V^{\mathrm{R.}}(r)$ and $V^{\mathrm{N.R.}}(r)$ coincide at large r region. On the other hand, at small r region, the difference between them becomes large as naturally expected, and the short distance differences of the potentials may contribute to reproducing nodal excited states.

Appendix B

— *Potential from a Gauge-Invariant Smeared Operator* —

As we showed, the obtained potentials exhibit a Coulomb plus linear behavior. However, potentials with different operators are generally different. Therefore, the Cornell-like behavior is not universal. Here, we show a potential with a different operator from that used in the main part.

The NBS amplitude with gauge-invariant smeared sink operators is defined by

$$\chi^{\mathrm{smr}}(\vec{x}+\vec{r},\vec{x},t-t_0;J^\pi) \equiv \langle 0|\,\bar{q}(\vec{x}+\vec{r},t)L(\vec{r},\vec{x},t;m)\Gamma q(\vec{x},t)\overline{\mathcal{J}}_{\bar{q}q}(t_0;J^\pi)\,|0\rangle\,,$$
$$L(\vec{r}=n\hat{\mu},\vec{x},t) \equiv U_\mu(\vec{x}+n\hat{\mu},t)\cdots U_\mu(\vec{x}+\hat{\mu},t)U_\mu(\vec{x},t). \qquad \text{(B·1)}$$

A schematic figure of the amplitude is shown in Fig. 7. The operator $L(\vec{r},\vec{x},t;m)$ constructed by link variables connects $\vec{x}$ and $\vec{x}+\vec{r}$ with a straight-line path. Here, the direction of $\vec{r}$ is chosen to be the x-, y-, or z-direction, i.e., on-axes.

Figure 8 shows a potential obtained from the smeared NBS amplitude, $V^{\mathrm{smr}}(r)$ (red points for V channel and blue points for PS channel), and that obtained in Coulomb gauge, $V^{\mathrm{Coul.}}(r)$ (green points for V channel and blue points for PS channel). Note that the data of $V^{\mathrm{smr}}(r)$ are only calculated on the points with integral multiples of the lattice spacing a, because $\vec{r}$ in Eq. (B·1) is on-axis. $V^{\mathrm{smr}}(r)$ shows the linear plus Coulomb behavior similar to that in Coulomb gauge, and, more over, the two potentials almost coincide. This fact shows that the gauge-invariant operator is also a suitable one for a constituent quark mass, and the Coulomb-gauge operator used in the main part is similar to the gauge-invariant operator of Eq. (B·1).

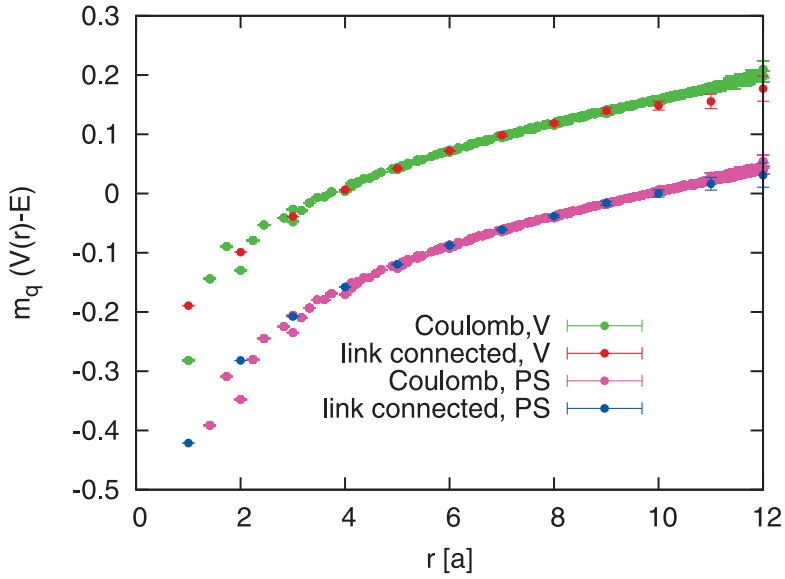

Fig. 8. Comparison of a potential with gauge-invariant smeared operator, $V^{\rm smr}(r)$, to that with Coulomb-gauge operator, $V^{\rm Coul.}(r)$. The red (blue) points are the data with gauge-invariant smeared operator in V (PS) channel, and the green (magenta) points are that in Coulomb gauge in V (PS) channel. The two potentials almost coincide.

References

1) C. B. Chiu, Ann. Rev. Nucl. Part. Sci. **22** (1972), 255.
2) G. S. Bali, Phys. Rep. **343** (2001), 1.
3) T. T. Takahashi, H. Matsufuru, Y. Nemoto and H. Suganuma, Phys. Rev. Lett. **86** (2001), 18.
   T. T. Takahashi, H. Suganuma, Y. Nemoto and H. Matsufuru, Phys. Rev. D **65** (2002), 114509.
4) E. Eichten, K. Gottfried, T. Kinoshita, K. D. Lane and T. M. Yan, Phys. Rev. D **21** (1980), 203.
5) T. Iritani, H. Suganuma and H. Iida, Phys. Rev. D **80** (2009), 114505.
6) N. Brambilla, A. Pineda, J. Soto and A. Vairo, Nucl. Phys. B **566** (2000), 275; Rev. Mod. Phys. **77** (2005), 1423.
7) L. S. Brown and W. I. Weisberger, Phys. Rev. D **20** (1979), 3239.
8) E. Eichten and F. L. Feinberg, Phys. Rev. Lett. **43** (1979), 1205.
9) Y. Koma and M. Koma, Nucl. Phys. B **769** (2007), 79.
10) S. Godfrey and N. Isgar, Phys. Rev. D **32** (1985), 189.
    R. Ricken et al., Eur. Phys. J. A **9** (2000), 221.
11) N. Ishii, S. Aoki and T. Hatsuda, Phys. Rev. Lett. **99** (2007), 022001.
12) S. Aoki, T. Hatsuda and N. Ishii, Prog. Theor. Phys. **123** (2010), 89.
13) H. Nemura, N. Ishii, S. Aoki and T. Hatsuda, Phys. Lett. B **673** (2009), 136.
14) H. Nemura et al. (HAL QCD and PACS-CS Collaboration), PoS(LAT2009)152.
15) K. Murano, N. Ishii, S. Aoki and T. Hatsuda, Prog. Theor. Phys. **125** (2011), 1225.
16) T. Inoue et al. (HAL QCD Collaboration), Prog. Theor. Phys. **124** (2010), 591.
17) T. Inoue et al. (HAL QCD Collaboration), Phys. Rev. Lett. **106** (2011), 162002.
18) T. Doi et al. (HAL QCD Collaboration), arXiv:1106.2276; PoS(Lattice 2010)136.
19) K. Sasaki et al. (HAL QCD Collaboration), PoS(Lattice 2010)157, arXiv:1012.5684.
20) Y. Ikeda et al. (HAL QCD Collaboration), arXiv:1002.2309; Prog. Theor. Phys. Suppl. No. 186 (2010), 228.
21) T. Kawanai and S. Sasaki, Phys. Rev. Lett. **107** (2011), 091601.

22) T. Hatsuda, arXiv:1101.1463.
23) T. T. Takahashi and Y. Kanada-En'yo, Phys. Rev. D **82** (2010), 094506.
24) W. Królikowski and J. Rzewuski, Nuovo Cim. **4** (1956), 1212.
25) M. M. Levy, Phys. Rev. **88** (1952), 725.
26) A. Klein, Phys. Rev. **90** (1953), 1101.
27) A. Klein and T.-S. H. Lee, Phys. Rev. D **10** (1974), 4308.
28) W. Macke, Phys. Rev. **91** (1953), 195.
29) Y. Ikeda and H. Iida, PoS(Lattice 2010)143.
30) G. Hohler et al., Nucl. Phys. B **114** (1976), 505.